Available online at www.sciencedirect.com
SCIENCE DIRECT®
Journal of Crystal Growth 274 (2005) 379–386
JOURNAL OF CRYSTAL GROWTH
www.elsevier.com/locate/jcrysgro

Flow and segregation control by accelerated rotation for vertical Bridgman growth of cadmium zinc telluride: ACRT versus vibration

C.W. Lan*

Department of Chemical Engineering, National Taiwan University, No. 1, Sec. 4, Roosevelt Rd, Taipei , Taiwan 10617, Republic of China

Received 27 October 2004; accepted 27 October 2004
Communicated by J.J. Derby
Available online 8 December 2004

Abstract

The control of flow and segregation by accelerated crucible rotation is investigated by computer simulation of vertical Bridgman crystal growth of cadmium zinc telluride. In view of the cycle frequency, two extremes, i.e., the accelerated crucible rotation technique (ACRT) and angular vibration technique (AVT), are investigated and compared. For a simple benchmark system, it is clear that ACRT generates significant oscillatory growth and segregation, while increasing slightly the global mixing. On the other hand, AVT provides, essentially, a steady control and can reverse easily the radial segregation without enhancing the global mixing. Although both techniques generate similar averaged flow structures and reduce radial segregation, AVT is more effective for growth control.

PACS: 44.25.+f; 47.27.Te; 81.10.Fq; 02.60.c6; 02.70Fj

Keywords: A1. Accelerated rotation; A1. Angular vibration; A1. Convection; A1. Segregation; B2. Bridgman method

1. Introduction

The control of convection and segregation is important in Bridgman crystal growth. Because of a lack of control over stirring conditions, the use of external forces is often adopted. Scheel and Schulz-DuBois proposed an accelerated crucible rotation technique (ACRT) to control the melt mixing [1]. By controlling the acceleration cycle, it is possible to control the melt mixing at either an enhanced mixing [2–4] or diffusion-limited mode [5]. The effects of ACRT also depend on the ratio of the melt depth to the size of Ekman cells, on the buoyancy convection, and on the vortices that sometimes form due to the Taylor–Görtler instability near the ampoule wall [6–8]. Particularly,

*Tel./fax: +886 2 2363 3917.
E-mail address: cwlan@ntu.edu.tw (C.W. Lan).

0022-0248/$ - see front matter © 2004 Elsevier B.V. All rights reserved.
doi:10.1016/j.jcrysgro.2004.10.059

ACRT is believed to be useful for the vertical Bridgman growth of cadmium zinc telluride (ZnCdTe), and has attracted extensive discussion recently [7–10]. Nevertheless, it is still controversial whether or not ACRT is the best means of growth control, because the issues of growth striations, radial, and axial segregations need to be judged carefully. In view of these observations, we believe that using computer simulations to perform a systematic comparison of ACRT to other means of convection control could provide useful information, reducing the need for crystal growers to undertake costly experiments.

The conventional approach to applying ACRT is to use a rotation cycle based on the time scale required to develop Ekman flow cells. The Ekman time scale is given by $R_C/\sqrt{\Omega\nu}$ [7], where R_C is the crystal radius, Ω the rotation speed, and ν the kinematic viscosity of the melt. For growth of ZnCdTe in small to medium vertical Bridgman systems, the Ekman time scale is up to tens of seconds. An alternative approach to applying ACRT is to use a cycle time that is much shorter than the Ekman time. This method is known as the angular vibration technique (AVT) [11]. In this technique, the ampoule is vibrated at high frequency (typically greater than 1 Hz) in the rotational direction to generate a radial outward Schlichting flow near the growth front. In a recent experimental and numerical study of a transparent system, the inversion of radial segregation by this technique was illustrated [11]. Pit formation due to local solute accumulation, a common occurrence in this system, was eliminated as well. Therefore, it is of interest to compare the two techniques applied to the well-studied ZnCdTe system.

There are also other control techniques based on ampoule vibration [12,13]. For example, the coupled vibrational stirring (CVS) method [12] uses asymmetric rotational motion, which generates flushing flow at the top melt surface and thus enhances solute mixing. Unfortunately, the vigorous global mixing generated by CVS is not favored for axial segregation control. To reduce axial segregation, global solute mixing needs to be minimized [6]. Moreover, an unstable growth rate was also observed in the CVS-controlled oxide growth [12].

In this paper, we take a simple model that has been extensively studied by Liu et al. [9] and Yeckel and Derby [8] using computer simulation. Since the calculated results are very different in these papers, our independent calculations provide a third reference for benchmarking of the system studied. Hence, prior to comparing ACRT to AVT, a benchmark comparison of our ACRT simulations with the previous calculations is presented. Then, the simulated results for AVT are compared to the time-averaged ACRT flow as well as to the case without rotation. Finally, the scalability issue is studied by doubling the system size in the simulation.

2. Model system and simulation

For benchmarking comparison, the vertical Bridgman growth system for ZnCdTe investigated by Yeckel and Derby [8] and Liu et al. [9] is considered. The schematic of the system is shown in Fig. 1, where the furnace profile (T_f) used by Liu et al. has been fitted using a polynomial by Yeckel and Derby:

$$T_f = T_m(0.9937 + 7.45\times10^{-3}x + 4.262\times10^{-4}x^2 + 1.221\times10^{-5}x^3 + 1.374\times10^{-6}x^4), \quad (1)$$

where T_m is the melting temperature and x the dimensionless axial distance normalized by the crystal radius (R_c). Growth is initiated by translating the thermal profile upward, with the position x related to the axial position z by $x = [(z - z_0) - V_f t]/R_c$, where z_0 is the initial reference position for $x = 0$, V_f the translation speed of the furnace, and t the growth time. The ampoule thickness is 2.5 mm, and the sample height is $L = 8.25$ cm for the benchmark system and $L = 16.25$ cm for the system after scaling up. Also, the temperatures at the crystal bottom and melt surface, as well as in the ampoule at the same height, are set to the furnace temperature there. The initial growth condition is set at $z_0 = 1$ cm for the benchmarking system and 3 cm for the large system; the translation speed of the thermal profile is 1×10^{-4} cm/s for all cases. Because the precise initial position of the melt-crystal interface is not known from the

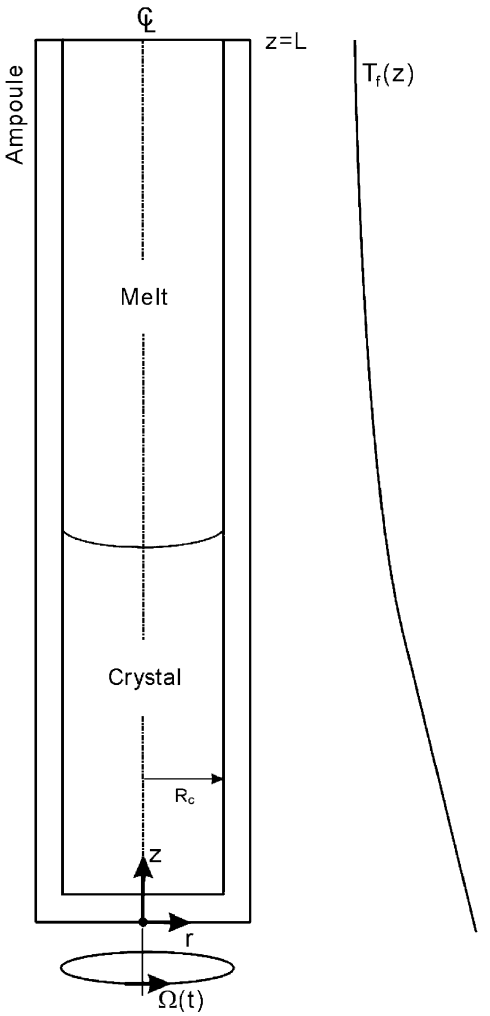

Fig. 1. Schematic of a vertical Bridgman system for ZnCdTe.

previous papers, we have adjusted the time at which ACRT is started such that the melt depth is approximately equal to the previously published simulations of this system. This gives the growth time of 18,000 s before ACRT is turned on. For the large system, ACRT starts at 36,000 s. The ACRT cycle is illustrated in Fig. 2, which is the same as the one used in [8,9]; the maximum rotation speed Ω is 30 rpm and the cycle period $P_{\mathrm{ACRT}} = 24$ s. The physical properties of ZnCdTe and related boundary conditions used in Ref. [8] are adopted.

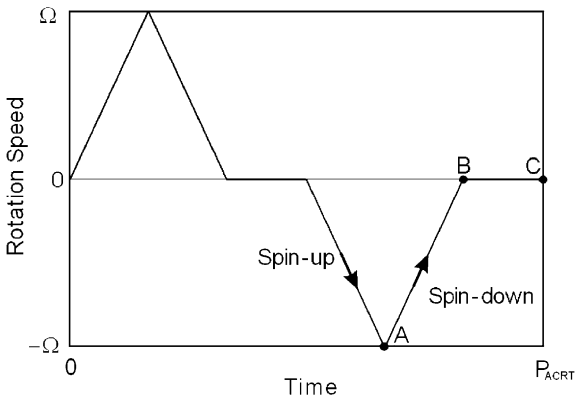

Fig. 2. ACRT rotation cycle; $P_{\mathrm{ACRT}} = 24$ s.

The governing equations and boundary conditions are discretized by a finite volume method, and the resultant differential/algebraic equations are solved by DASPK solver with adaptive stepsize control [14]. For benchmark comparison, the results are also presented after completion of 100 ACRT cycles. The total number of unknowns after the finite volume approximation is 34,052, and all the calculations are performed using a personal computer (P4-3 GHz CPU).

For angular vibration, the velocity boundary condition at the solidification front is similar to that for ACRT but having a sinusoidal cycle:

$$v_\theta = b_v \omega r \sin \omega t, \tag{2}$$

where v_θ is the angular velocity, b_v the vibration amplitude (a fraction of 2π), and ω the angular frequency, which is related to the vibration frequency f by $\omega = 2\pi f$. Also, r is the radial distance and t the time. Compared with ACRT, $b_v\omega$ is equivalent to the maximum rotation speed Ω. However, direct numerical simulation using this boundary condition is not realistic due to the small stepsize and long simulation time required. An easier approach for simulation is to find an effective boundary condition similar to that used in the Schlichting flow [13]. It can be obtained by using the Nyborg formula [15,16] that the tangential velocity at the solidification front can be replaced by a slip boundary condition :

$$v_t = \frac{\pi}{2} b_v^2 f r \sin \phi, \tag{3}$$

where ϕ the angle between the tangent of the growth front and the growth axis. However, Eq. (3) is valid only when the frequency is sufficiently high, so that the Schlichting layer thickness, i.e., $\sim \sqrt{\nu/\pi f}$, is small as compared with the domain size for convection. For $f = 60$ Hz, the Schlichting boundary layer thickness is about 4.7×10^{-2} mm in the system studied here. Accordingly, Eq. (3) gives a good approximation of the effective boundary layer on the bulk flow. For $b_v = 0.04$, the vibration is equivalent to an ACRT having maximum rotation speed 905 rpm and period 1/60 s. In other words, the external force applied to the system is quite substantial. We have also carried out direct numerical simulation to examine this approximation, and the agreement is quite good if the frequency is greater than 5 Hz.

3. Results and discussion

Before the comparison of ACRT and AVT, the calculated results for ACRT are compared with the ones reported by Yeckel and Derby [8] for the case under normal gravity. Fig. 3 shows the calculated flow patterns and concentration contours in the 101th ACRT cycle. The zinc concentration C has been normalized by the initial concentration C_0; $C_0 = 0.04$ (mole fraction). These calculated results correspond to the indicated points illustrated in Fig. 2, where A is the end of the spin-up, B the end of the spin-down, and C the beginning of the spin-up period. As shown in Fig. 3a, after spinning up, there is a counterclockwise flow induced, and the flow intensity is $-8.721 \times 10^{-3}\,\mathrm{cm^3/s}$, which is in good agreement with the one in Ref. [8] ($-8.72 \times 10^{-3}\,\mathrm{cm^3/s}$). It should be pointed out that the figure captions for Figs. 2 and 3 in Ref. [8] were swapped accidentally. Therefore, the comparison of the values for stream function (Ψ) refers to the values in Fig. 2 of Ref. [8]. Similarly, at the end of the spin-down cycle (Fig. 3b) the lower cell becomes clockwise and the flow intensity is $5.932 \times 10^{-3}\,\mathrm{cm^3/s}$, while the upper cell is counterclockwise having the intensity of $-5.03 \times 10^{-3}\,\mathrm{cm^3/s}$. Again 5.88×10^{-3} and $-5.03 \times 10^{-3}\,\mathrm{cm^3/s}$, respectively, were reported in Ref. [8]. At the beginning of spinning up, the flow

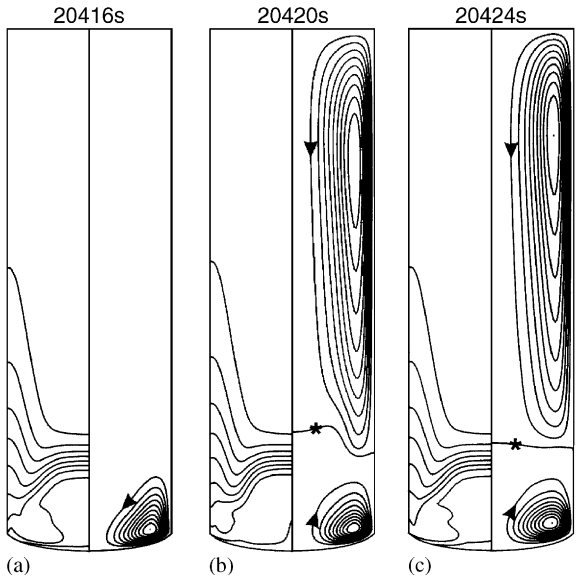

Fig. 3. Calculated flow (right) and Zn concentration (left) fields in the 101th ACRT cycle: (a) $t = 20416$ s (point A in Fig. 2); (b) $t = 20420$ s (point B in Fig. 2); (c) $t = 20424$ s (point C in Fig. 2). $\Psi_{min} = -8.721 \times 10^{-3}\,\mathrm{cm^3/s}$, $\Psi_{max} = 0\,\mathrm{cm^3/s}$, $C_{min}/C_0 = 0.837$, $C_{max}/C_0 = 0.9461$ in (a), $\Psi_{min} = -5.026 \times 10^{-4}\,\mathrm{cm^3/s}$, $\Psi_{max} = 5.932 \times 10^{-3}\,\mathrm{cm^3/s}$, $C_{min}/C_0 = 0.8149$, $C_{max}/C_0 = 0.9605$ in (b), and $\Psi_{min} = -5.608 \times 10^{-4}\,\mathrm{cm^3/s}$, $\Psi_{max} = 3.474 \times 10^{-3}\,\mathrm{cm^3/s}$, $C_{min}/C_0 = 0.8370$, $C_{max}/C_0 = 0.94602$ in (c). The asterisks (*) indicate the zero streamfunction.

structure remains unchanged, as shown in Fig. 3c, but the flow intensities are reduced to 3.474×10^{-3} and $-5.608 \times 10^{-4}\,\mathrm{cm^3/s}$ (3.46×10^{-3} and $-5.45 \times 10^{-4}\,\mathrm{cm^3/s}$ in Ref. [8]), respectively, for the lower and the upper cells. The quantitative comparison of concentration fields is difficult due to the lack of information on the initial melt/crystal interface position and maximum and minimum values in Ref. [8]. However, our concentration distributions are very similar to the reported ones. Furthermore, the agreement on the interface shape is very good.

The calculated results without ACRT at the same time as that for Fig. 3c ($t = 20424$ s) are shown in Fig. 4a. This two-cell flow structure is a typical one for vertical Bridgman growth. The lower flow cell is induced by the interface deflection, largely caused in this system by the release of latent heat, while the upper cell is due to the non-uniform heating. Because the flow in

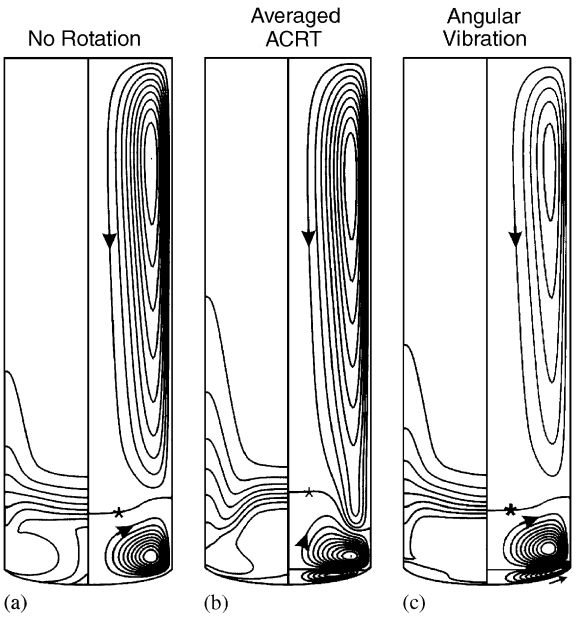

Fig. 4. Calculated flow (right) and Zn concentration (left) fields at $t = 20424$ s: (a) without rotation; (b) time-averaged ACRT solution; (c) with angular vibration ($b_v = 0.04$ at 60 Hz). $\Psi_{min} = -5.592 \times 10^{-4}\,cm^3/s$, $\Psi_{max} = 2.252 \times 10^{-3}\,cm^3/s$, $C_{min}/C_0 = 0.8036$, $C_{max}/C_0 = 0.9482$ in (a), $\Psi_{min} = -5.369 \times 10^{-4}\,cm^3/s$, $\Psi_{max} = 1.054 \times 10^{-3}\,cm^3/s$, $C_{min}/C_0 = 0.8417$, $C_{max}/C_0 = 0.9497$ in (b), and $\Psi_{min} = -1.015 \times 10^{-3}\,cm^3/s$, $\Psi_{max} = 1.975 \times 10^{-3}$ cm3/s, $C_{min}/C_0 = 0.8295$, $C_{max}/C_0 = 0.9481$ in (c).

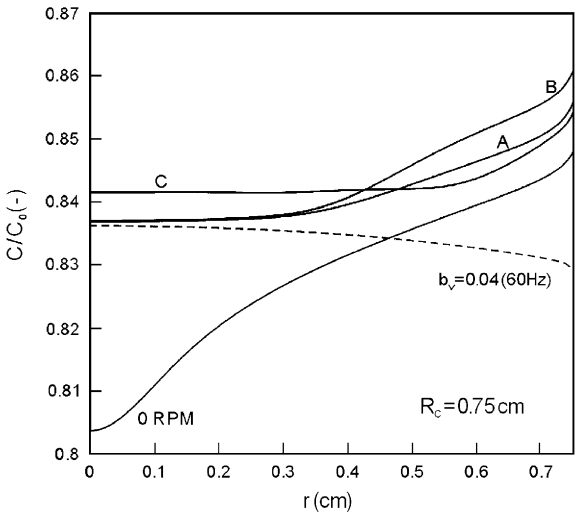

Fig. 5. Calculated radial segregation for different growth conditions; the zinc concentrations in the melt along the interface are taken for illustration.

Fig. 4a is steady, for better comparison we calculate the time average of the flow and concentration fields over the 101th cycle of ACRT, as illustrated in Fig. 4b. As shown, time-averaging reveals a three-cell flow structure. The lowest cell apparently is due to the crucible acceleration. Interestingly, by vibrating the ampoule at 60 Hz ($b_v = 0.04$) we have obtained a flow structure in Fig. 4c that is similar to the averaged one of ACRT in Fig. 4b. The vibration generates a radial outward streaming flow near the growth front. Because of this flow, the radial segregation, as shown in Fig. 5, can be reversed. Without rotation, the zinc concentration is lower at the center of the interface. ACRT reduces the radial concentration difference, as labeled by A, B, and C, respectively, corresponding to the points indicated in Fig. 2. The change in concentration profile with rotation speed during ACRT could be the cause for growth striations. On the other hand, the angular vibration essentially gives a steady radial concentration profile. With a smaller vibration amplitude or frequency, it is possible to have an even more uniform distribution. It should be pointed out that the uniformity on the wafer obtained from the crystal is not the same as the uniformity along the interface. The effect of interface shape and axial segregation needs to be taken into account. In the present case, a slightly higher zinc concentration at the center (the last part in a given wafer to freeze) is preferred because the present interface is concave and the segregation coefficient of zinc is greater than unity there.

The control of axial segregation is also important in Bridgman crystal growth. Fig. 6 shows the spatially averaged axial segregation (over the radial distance along the growth interface) for different conditions; $\overline{C_c}$ is the spatially averaged zinc concentration along the growth interface in the crystal and the interface position is also a spatial average. To illustrate significant axial segregation, simulation time is carried out up to 36,000 s having the solidification fraction of 0.4. As shown in Fig. 6, ACRT seems to slightly enhance the global mixing, so that its segregation behavior is slightly shifted toward the complete-mixing curve. Because the period is only 24 s, one

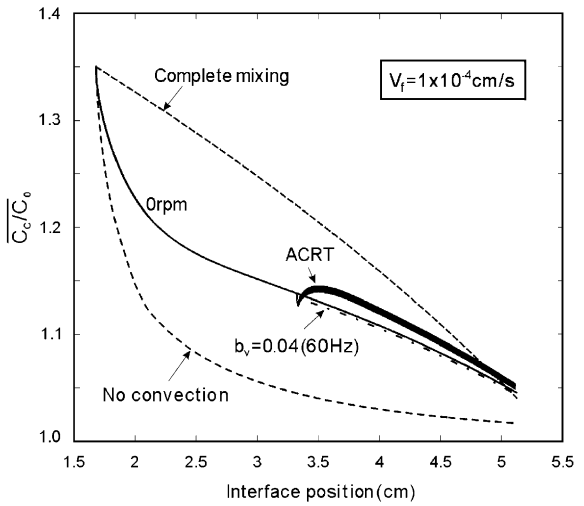

Fig. 6. Calculated spatially averaged (over the radial distance) zinc concentrations in the crystal along the radially averaged growth distance for different growth conditions.

cannot distinguish the oscillation period from the curve. However, the amplitude of the oscillation can be seen from the bandwidth of the curve. On the other hand, the angular vibration slightly reduces the mixing; the segregation for the case without rotation is included for reference. As just mentioned, to reduce the axial segregation, the global mixing needs to be reduced. The no-convection (diffusion-controlled) limit is also illustrated to show the largest possible reduction of the axial segregation. In other words, if the system length is sufficiently long, the axial segregation after the initial diffusion period (about 1–2 cm here) is leveling off, as indicated by the no-convection curve from the interface position of 4 cm in Fig. 6 to the end of solidification.

Another problem due to ACRT is the oscillatory growth speed. As pointed out before [7,17], remelting can occur when ACRT is applied to vertical Bridgman systems. To illustrate this, the growth rates at the centerline for the growth time up to 36,000 s are illustrated in Fig. 7a. As shown, the local growth rate oscillation due to ACRT is not trivial, but no back melting is observed at $r = 0$ for the ACRT cycle shown in Fig. 2. However, if we take one cycle period for illustration, as shown in Fig. 7b, one can see obvious back melting near the ampoule wall at the end of the spin-down

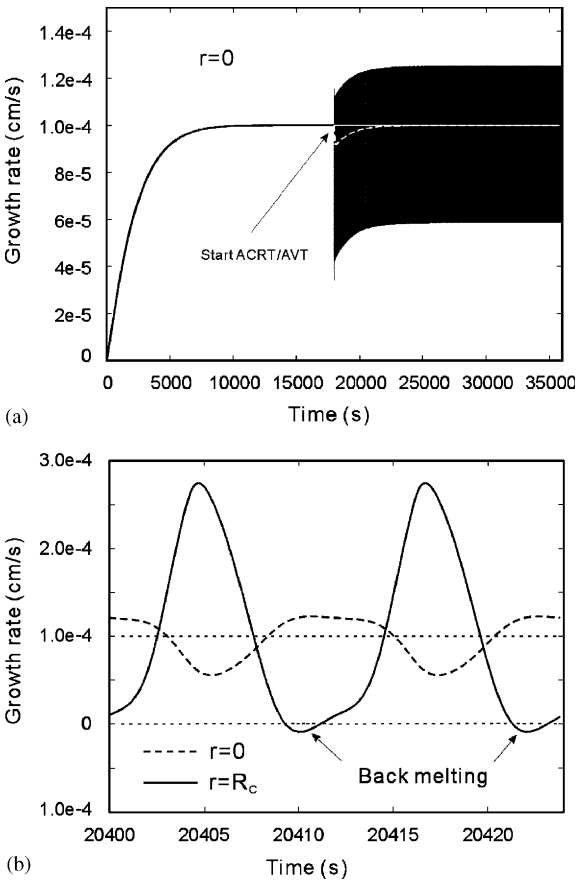

Fig. 7. (a) Calculated growth rate at the centerline for different growth conditions; the white dashed line is for the angular vibration; (b) growth rate at $r = 0$ and $r = R_c$ for ACRT in the 101th ACRT cycle. ACRT and ART start at $t = 18000$ s.

period, where the hotter melt is brought from the ampoule wall to the melt center along the growth interface. On the contrary, the angular vibration allows a steady growth rate to be reached quickly. The simulation for a cycle period of 48 s is also carried out and the results are similar.

The system studied by Liu et al. [9] and Yeckel and Derby [8] is smaller than typical industrial systems for ZnCdTe, which often have a crystal radius of several centimeters. In order to show that the same conclusions could be drawn for a practical system, numerical simulation is also carried out for a larger system, where the system size is doubled; the cycle period for ACRT is kept the same at 24 s. Fig. 8 shows the calculated results

at the 101th ACRT cycle for the large system ($R_c = 1.5$ cm and $L = 16.25$ cm). Again, the simulation times correspond to the points shown in Fig. 2. As shown, the overall flow structure and concentration fields remain similar to those in Fig. 3. However, the flow seems to be more complicated and smaller secondary cells are induced. The results without rotation are shown in Fig. 9a. The overall flow structure and concentration field are similar to those in Fig. 4a. The time-averaged flow and concentration fields in Fig. 9b are also similar to those in Fig. 4b for the ACRT case. Likewise, the flow and concentration fields in Fig. 9c are similar to those in Fig. 4c for the angular vibration case. Further comparison of the radial segregation in Fig. 10 gives a similar picture. Again, the melt concentrations along the interface are illustrated here. As shown, the ACRT indeed reduces significantly the radial segregation as compared with the case of no rotation.

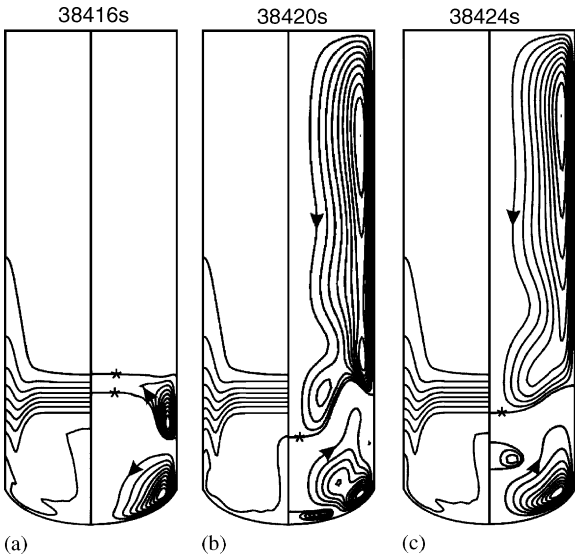

Fig. 8. Calculated flow (right) and zinc concentration (left) fields in the 101th ACRT cycle for the large system ($R_c = 1.5$ cm, $L = 16.25$ cm): (a) $t = 38416$ s (point A in Fig. 2); (b) $t = 38420$ s (point B in Fig. 2); (c) $t = 38424$ s (point C in Fig. 2). $\Psi_{min} = -6.25 \times 10^{-2}$ cm^3/s, $\Psi_{max} = 8.965 \times 10^{-4}$ cm^3/s, $C_{min}/C_0 = 0.8181$, $C_{max}/C_0 = 0.9695$ in (a), $\Psi_{min} = -1.122 \times 10^{-3}$ cm^3/s, $\Psi_{max} = 2.447 \times 10^{-2}$ cm^3/s, $C_{min}/C_0 = 0.8177$, $C_{max}/C_0 = 0.9695$ in (b), and $\Psi_{min} = -1.231 \times 10^{-3}$ cm^3/s, $\Psi_{max} = 2.362 \times 10^{-2}$ cm^3/s, $C_{min}/C_0 = 0.8179$, $C_{max}/C_0 = 0.9695$ in (c).

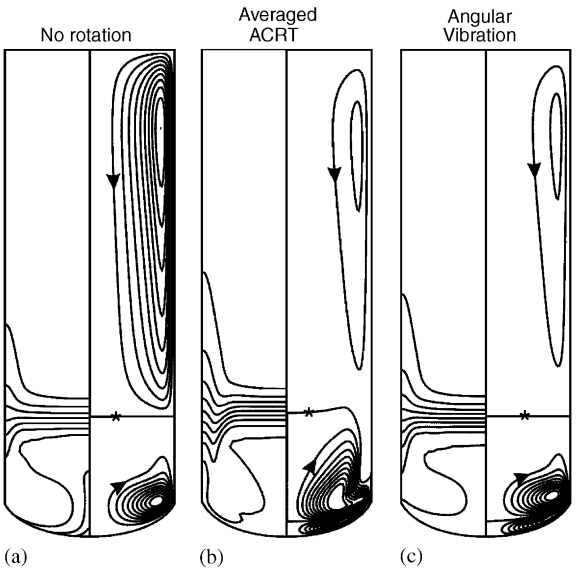

Fig. 9. Calculated flow (right) and zinc concentration (left) fields at $t = 38424$ s for the large system ($R_c = 1.5$ cm, $L = 16.25$ cm): (a) without rotation; (b) averaged ACRT solution at the 101th cycle; (c) with angular vibration ($b_v = 0.04$ at 60 Hz). $\Psi_{min} = -1.24 \times 10^{-3}$ cm^3/s, $\Psi_{max} = 1.634 \times 10^{-2}$ cm^3/s, $C_{min}/C_0 = 0.7699$, $C_{max}/C_0 = 0.9695$ in (a), $\Psi_{min} = -5.215 \times 10^{-3}$ cm^3/s, $\Psi_{max} = 4.002 \times 10^{-3}$ cm^3/s, $C_{min}/C_0 = 0.8222$, $C_{max}/C_0 = 0.9719$ in (b), and $\Psi_{min} = -5.376 \times 10^{-3}$ cm^3/s, $\Psi_{max} = 1.450 \times 10^{-2}$ cm^3/s, $C_{min}/C_0 = 0.8134$, $C_{max}/C_0 = 0.9695$ in (c).

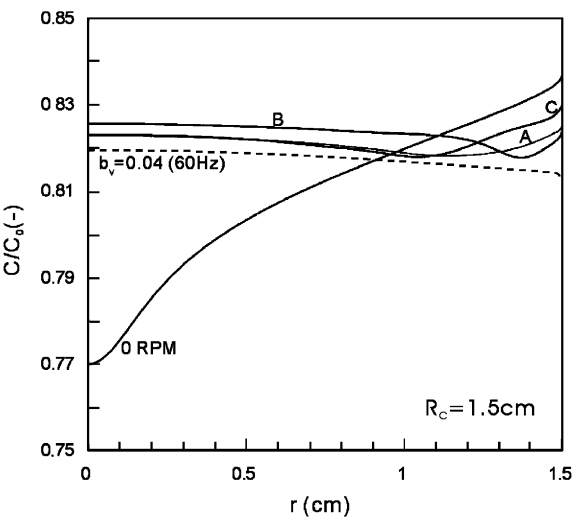

Fig. 10. Calculated radial zinc distribution in the melt along the growth interface for the larger system at different growth conditions.

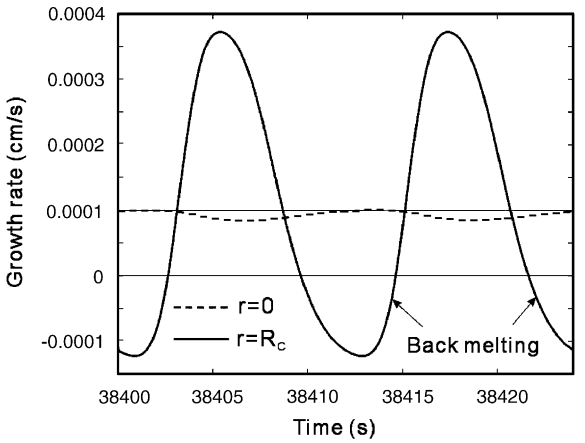

Fig. 11. Calculated growth rate for the larger system at $r = 0$ and $r = R_c$ for ACRT in the 101th ACRT cycle.

However, angular vibration can reduce the radial segregation even further.

The oscillatory growth rate in the 101th cycle of ACRT is shown in Fig. 11. As shown, the back melting near the ampoule wall at the end of the spin-down period becomes more serious than observed in the smaller system. Clearly, with the same rotation speed, the amplitude of the growth rate oscillation near the ampoule wall increases for a larger system.

4. Conclusions

We have performed some simulations using a benchmark growth system of ZnCdTe considering two extreme cases of ACRT in terms of the cycle period. For the typical ACRT having a rotation period based on the Ekman time scale, our calculated results are in good agreement with the results reported by Yeckel and Derby [8]. Therefore, these results could be useful for future benchmarking in crystal growth modeling. From the calculated results, it is clear that ACRT cycle studied here is useful in reducing radial segregation. For a small-scale system, the ACRT cycle studied here does not introduce much global mixing. As pointed out by Yeckel and Derby [8], this is simply due to the upper buoyancy cell that inhibits the penetration of the spin-down flow to the bulk melt. On the other hand, we have also shown that angular vibration, essentially an ACRT using a very small cycle period, makes the growth slightly more diffusive. This reduction of the global mixing is also due to the cell-stacking; the buoyancy cell stacks upon the Schlichting cell. More importantly, reversing radial segregation can be easily achieved by angular vibration. Also, the flow and concentration fields, as well as the growth rate, seem to be stable at high frequency. Similar results are observed in a system that is doubled in size.

Acknowledgments

The author is grateful to Dr. A. Yeckel and Prof. J.J. Derby for providing their original simulation data for comparison. The valuable discussion with them and Prof. T.P. Lyubimova is highly appreciated.

References

[1] H.J. Scheel, E.O. Schulz-Dubois, J. Crystal Growth 8 (1971) 304.
[2] P. Capper, J.J.G. Gosney, C.L. Jones, J. Crystal Growth 70 (1984) 356.
[3] W.G. Coates, P. Capper, C.L. Jones, J.J.G. Gosney, C.K. Ard., I. Kenworthy, A. Clark, J. Crystal Growth 94 (1989) 959.
[4] P. Capper, J.C. Brice, C.L. Jones, W.G. Coates, J.J.G. Gosney, C.K. Ard., I. Kenworthy, J. Crystal Growth 89 (1988) 171.
[5] P. Capper, J.J. Gosney, UK Patent 2098879A, 1982.
[6] J.C. Brice, Crystal Growth Processes, Wiley, New York, 1986.
[7] A. Yeckel, J.J. Derby, J. Crystal Growth 209 (2000) 734.
[8] A. Yeckel, J.J. Derby, J. Crystal Growth 233 (2001) 599.
[9] X. Liu, W. Jie, Y. Zhou, J. Crystal Growth 219 (2000) 22.
[10] X. Liu, W. Jie, Y. Zhou, J. Crystal Growth 209 (2000) 751.
[11] W.C. Yu, Z.B. Chen, W.T. Hsu, B. Roux, T.P. Lyubimova, C.W. Lan, J. Crystal Growth 271 (2004) 474.
[12] K.T. Zawilski, M. Claudia, C. Custodio, R.C. DeMattei, R.S. Feigelson, J. Crystal Growth 258 (2003) 211.
[13] G.Z. Gershuni, D.V. Lyubimov, Thermal Vibration Convection, Wiley, New York, 1998.
[14] C.W. Lan, M.C. Liang, J. Crystal Growth 186 (1998) 187.
[15] W.L. Nyborg, Acoustic Streaming, in: W.P. Mason (Ed.), Physical Acoustics, Academic Press, New York, 1965.
[16] T.P. Lyubimova, private communication.
[17] C.W. Lan, J.H. Chian, J. Crystal Growth 203 (1999) 286.